PHYSICAL REVIEW C **83**, 064603 (2011)

Experimental study of ^{6}He + ^{9}Be elastic scattering at low energies

K. C. C. Pires,* R. Lichtenthäler, A. Lépine-Szily, V. Guimarães, P. N. de Faria, A. Barioni, D. R. Mendes Junior, V. Morcelle, R. Pampa Condori, M. C. Morais, J. C. Zamora, and E. Crema
Departamento de Física Nuclear, Universidade de São Paulo, C.P. 66318, 05389-970, São Paulo, Brazil

A. M. Moro
Departamento de FAMN, Facultad de Física, Universidad de Sevilla, Apdo. 1065, E-41080 Sevilla, Spain

M. Rodríguez-Gallardo
Instituto de Estructura de la Materia, CSIC, Serrano 123, E-28006 Madrid, Spain
Departamento de FAMN, Facultad de Física, Universidad de Sevilla, Apdo. 1065, E-41080 Sevilla, Spain

M. Assunção
Departamento de Ciências Exatas e da Terra, Universidade Federal de São Paulo, Campus Diadema, São Paulo, Brazil

J. M. B. Shorto
Instituto de Pesquisas Energéticas e Nucleares (IPEN-CNEN), Comissão Nacional de Energia Nuclear, São Paulo, Brazil

S. Mukherjee
Physics Department, Faculty of Science, The M.S. University of Baroda, Vadodara, India
(Received 11 February 2011; published 13 June 2011)

New data for the ^{6}He + ^{9}Be reaction at $E_{\rm lab} = 16.2$ and 21.3 MeV have been taken and analyzed. The effect of the collective couplings to the excited states of the target has been studied by means of coupled-channels calculations, using a double-folding potential for the bare interaction between the colliding nuclei, supplemented with a phenomenological imaginary part of Woods-Saxon type. In addition, three- and four-body continuum-discretized coupled-channels calculations have been performed to investigate the effect of the projectile breakup on the elastic scattering. Both effects, the coupling to target and projectile excited states, are found to affect significantly the elastic scattering. The *trivial local polarization* potential extracted from the continuum-discretized coupled-channels calculations indicates that continuum couplings produce a repulsive real part and a long-range imaginary part in the projectile-target interaction.

DOI: 10.1103/PhysRevC.83.064603 PACS number(s): 24.10.Eq, 24.50.+g, 25.60.Bx, 29.38.−c

I. INTRODUCTION

Since the early nineties, the ^{6}He nucleus has attracted much attention due to its halo and Borromean structure. With the aim of understanding this peculiar structure and its influence on the scattering observables, a considerable amount of experimental data of ^{6}He-induced reactions on a variety of targets has been accumulated over the past years. Depending on the energy regime and the target mass, the loosely bound structure manifests in different ways. For medium-mass and heavy targets, and for energies around the Coulomb barrier, the differential elastic cross section exhibits a smooth angular dependence, with a partial or complete suppression of the Fresnel oscillations that characterizes the scattering of heavy ions at low energies. To reproduce this behavior using an optical potential, one requires an imaginary part of long range [1–4]. This *long-range absorption* effect suggests the presence of reaction channels that remove flux from the elastic channel at distances well beyond the strong absorption radius, in contrast to the picture suggested by the strong absorption model. Continuum-discretized coupled-channels (CDCC) calculations using either a simplified *dineutron* model [5,6] or a more realistic three-body model for the ^{6}He nucleus [4,7–11] indicate that this long-range absorption phenomenon can be explained in terms of the strong couplings to the breakup channels due mainly to the dipole Coulomb interaction.

As the mass of the target decreases, the dipole Coulomb effects are expected to become less and less important and, conversely, nuclear effects will gain importance. Coupling to breakup channels due to the nuclear interaction have been found in the past to affect also the elastic scattering of weakly bound systems, such as deuterons [12,13], ^{6}Li [14], or ^{11}Be [15], among others.

For ^{6}He, the existing data are more scarce. Ostrowski *et al.* [16] reported elastic and transfer data for ^{6}He + ^{12}C at 5.9 MeV, which were later analyzed by Krouglov and von Oertzen [17] within the coupled-reaction channels (CRC) formalism to investigate the $2n$ transfer channels populating several states of the ^{14}C residual nucleus. Milin *et al.* [18] measured the same reaction at a higher energy ($E_{\rm lab} = 18$ MeV) with the goal of extracting spectroscopic information of stretched neutron configurations in the ^{14}C final nucleus. Smith *et al.* [19] measured ^{6}He + ^{197}Au,

*kelly@dfn.if.usp.br

^{nat}Ti, ^{27}Al, ^{nat}C, ^{9}Be at $E_{lab} = 8.8$–9.3 MeV to deduce optical model parameters for the ^{6}He elastic scattering. Tao *et al.* [20] measured the ^{6}He + ^{9}Be quasielastic scattering at $E = 25$ MeV/A, and in addition to the angular distribution, a phenomenological optical potential was obtained. Lukyanov *et al.* [21] have performed calculations of microscopic optical potentials to analyze the ^{6}He + p elastic scattering data at $E_{lab} = 41.6$ MeV. Benjamim *et al.* [22] measured the ^{6}He + ^{27}Al reaction at four energies slightly above the Coulomb barrier ($E_{lab} = 9.5$–13.4 MeV). The reduced reaction cross section was found to be similar to that obtained for ^{6}Li + ^{27}Al at nearby energies.

More recently, Majer *et al.* [23] have measured the ^{6}He + ^{9}Be reaction at 16.8 MeV, reporting results for the elastic and two-neutron transfer channels. The differential elastic cross section was found to follow a pattern similar to that of ^{6}Li + ^{9}Be data at roughly the same energy. CDCC calculations reproduced satisfactorily the data and confirmed the importance of projectile breakup effects for light targets.

These works suggest that the scattering of ^{6}He on light targets exhibits common features to other weakly bound nuclei and, in particular, to ^{6}Li. This is in contrast to the case of the scattering by heavy targets where ^{6}He and ^{6}Li behave in a very different way, due to the strong Coulomb polarization experienced by the former.

In this work we present new experimental data for the ^{6}He + ^{9}Be reaction at two different energies, $E_{lab} = 16.2$ and 21.3 MeV. Besides the elastic data, the experiment showed a large yield of α particles, presumably coming from the projectile breakup or transfer to target states. Here, we focus on the elastic scattering data, performing a detailed analysis in terms of the CDCC method, with the goal of studying the role of the coupling to the continuum states of the projectile. In addition, we have performed coupled-channels (CC) with collective form factors, aimed at investigating explicitly the role of the target reorientation and its coupling to the low-lying collective states. These effects have been found to play a major role in the elastic and inelastic scattering of ^{6}Li + ^{9}Be at similar energies [24] and, consequently, they are likely to be important also in the present case.

The paper is structured as follows. In Sec. II, we describe the details of the experiment. In Sec. III, we present the theoretical analysis of the data within the CC and CDCC formalisms. For the latter, we consider two alternative models of ^{6}He, a simplified two-body (*dineutron*) model and a more realistic three-body model. Finally, in Sec. IV we summarize the main conclusions of this work.

II. EXPERIMENT

The ^{6}He + ^{9}Be measurements have been performed using the RIBRAS facility [25] of the Institute of Physics of the University of São Paulo, Brazil [26,27]. The ^{6}He beam was produced by the ^{9}Be(^{7}Li,^{6}He)^{10}B reaction with a 12-μm ^{9}Be foil and a 200-nAe ^{7}Li primary beam of 22.18 and 26.10 MeV. A tungsten Faraday cup suppresses the primary beam and measures its current during the experiment. In those conditions, the ^{6}He secondary beam intensity was of about 10^{4} pps. The RIBRAS system consists of two identical superconducting solenoids in line, which are able to select and focus light secondary beams up to energies of $E \approx 10$ MeV/A. In the present experiment only the first solenoid was used, and the ^{6}He particles were focused in the midway scattering chamber located between the two solenoids. A picture and a scheme of this system are shown in Fig. 1.

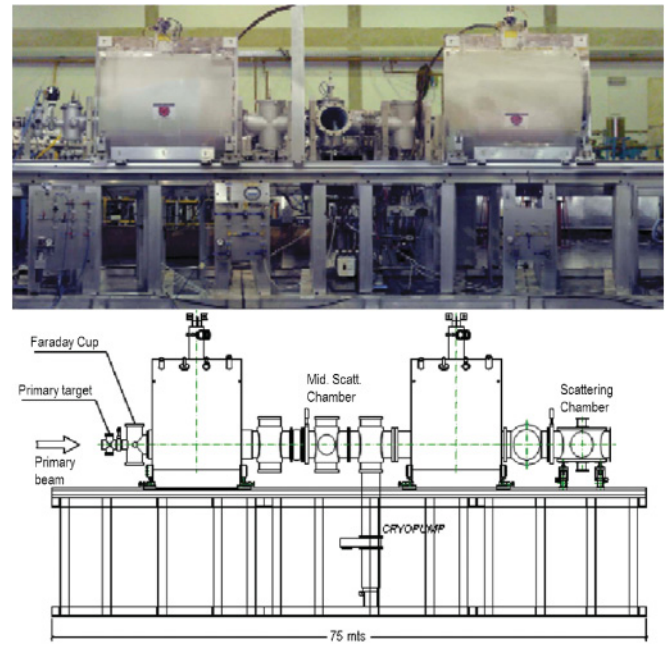

FIG. 1. (Color online) RIBRAS facility installed in the 45B Pelletron beam line.

The detection system consisted of four ΔE-E telescopes formed by silicon detectors with 20 and 1000 μm thickness, respectively, which provide the charge and mass identification of the ions coming out from the secondary target. The telescopes were mounted on both sides ($\theta > 0$ and $\theta < 0$) with respect to the secondary beam direction, allowing measurements at symmetric scattering angles ($\pm\theta$) to check the beam alignment. ^{9}Be and ^{197}Au secondary targets with 1.93 and 2.95 mg/cm^{2}, respectively, were used. The ^{197}Au target was used to monitor the secondary beam intensity during the experiment since the ^{6}He + ^{197}Au cross section is pure Rutherford at the energies and angles of this experiment. Each run with ^{9}Be target was followed by another run with ^{197}Au target, to measure the ^{6}He production rate. Initially, the secondary beam was focused directly in a telescope placed at zero degrees, using a faint primary beam (≈0.1–0.5 nAe). This procedure should reduce the effect of the intrinsic angular divergence ($\theta_{lab} = 1.5^{\circ}$–$4.5^{\circ}$) of the secondary beam as can be seen in Fig. 2.

The ^{6}He production rate was maximized by varying the solenoid current and measuring the number of ^{6}He particles produced at zero degrees.

Typical E-ΔE biparametric spectra obtained during the experiment, using ^{9}Be and ^{197}Au targets, are shown in Fig. 3. One sees the ^{6}He peak clearly separated from the ^{4}He and ^{7}Li^{2+} contaminants. It is interesting to observe the presence of a large yield of low-energy ^{4}He and ^{6}He particles that are produced in the ^{9}Be and are not present with the ^{197}Au target.

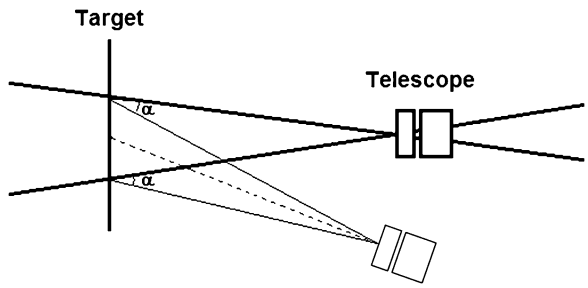

FIG. 2. Scheme of the procedure used to mitigate the effect of the beam divergence.

Those strips of low-energy events are possibly produced by the breakup of the projectile ^{6}He and target ^{9}Be due to their low breakup threshold of 0.973 and 1.65 MeV, respectively.

The elastic cross sections have been obtained by normalization with the ^{197}Au runs as described below:

$$\frac{\sigma^{^6\mathrm{He}+^9\mathrm{Be}}}{\sigma_R^{^6\mathrm{He}+^9\mathrm{Be}}} = \frac{\sigma^{^6\mathrm{He}+^{197}\mathrm{Au}}}{\sigma_R^{^6\mathrm{He}+^9\mathrm{Be}}} \frac{N_c^{\mathrm{Be}}}{N_c^{\mathrm{Au}}} \frac{J^{\mathrm{Be}}}{J^{\mathrm{Au}}} \left(\frac{N_b^{\mathrm{Au}}}{N_b^{\mathrm{Be}}}\right) \frac{N_t^{\mathrm{Au}}}{N_t^{\mathrm{Be}}}, \qquad (1)$$

where N_c^{Be} stands for the number of counts in the $^6\mathrm{He} + {}^9\mathrm{Be}$ peak at a given angle. N_c^{Au} is the sum of the number of counts of the ^{6}He $+^{197}$Au peaks of two adjacent runs of the same telescope at the same scattering angles, performed just before and after each ^{9}Be run as mentioned above, and $N_b^{\mathrm{Au}}/N_b^{\mathrm{Be}}$ is the ratio between the Faraday cup current integrators of the ^{197}Au runs (summed) and the ^{9}Be run. $\sigma_R^{\mathrm{Be,Au}}$ represents the calculated Rutherford cross section in the central angle of the detector, and J is the Jacobian of the transformation from the laboratory to center-of-mass frame. N_t is the target thickness (in atoms/cm^2), measured off-line by energy loss using an ^{241}Am α source. With this method, the $^6\mathrm{He} + {}^9\mathrm{Be}$ angular distribution becomes normalized and independent of the solid angle of the telescopes.

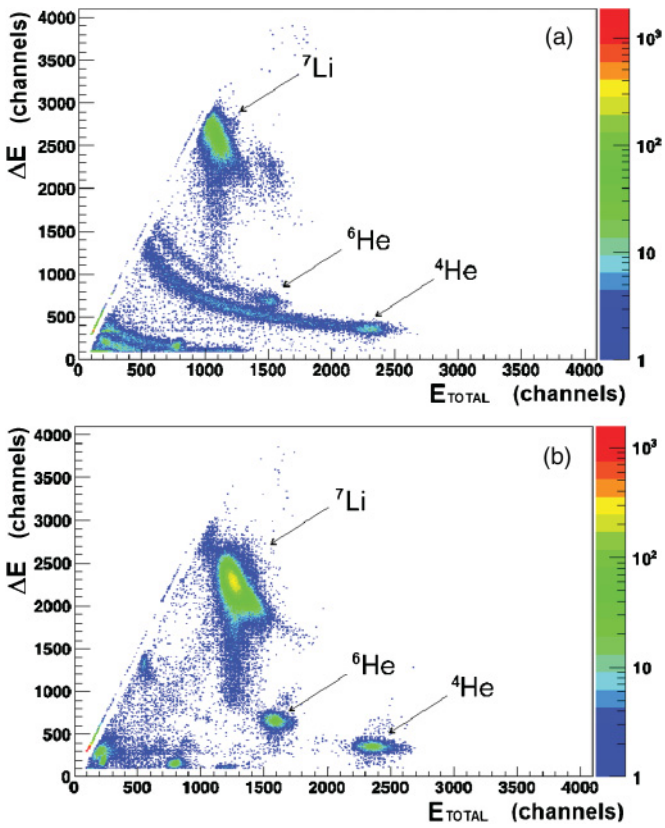

FIG. 3. (Color online) Biparametric spectrum obained with ^{6}He beam and (a) ^{9}Be and (b) ^{197}Au targets at $\theta_{\mathrm{lab}} = 15^\circ$.

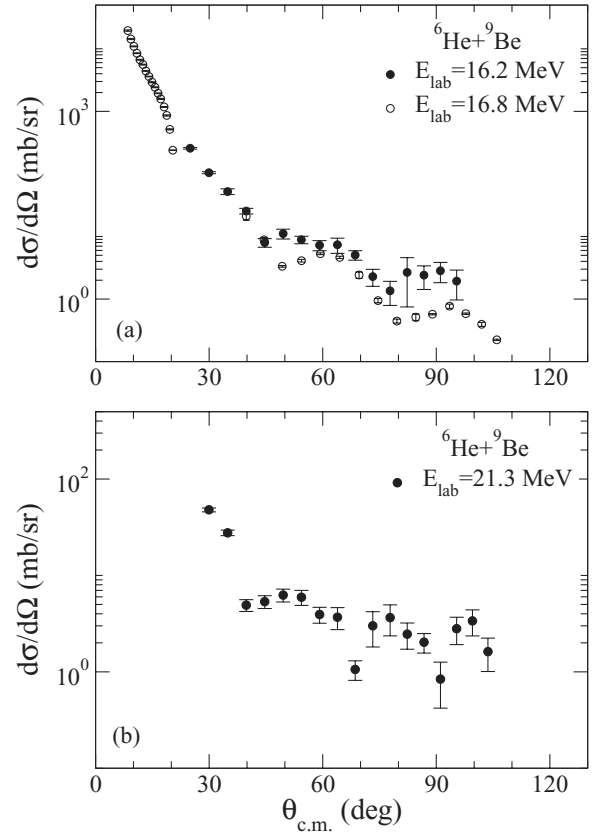

FIG. 4. Absolute differential cross sections for the $^6\mathrm{He} + {}^9\mathrm{Be}$ elastic scattering. The solid circles are the data from the present experiment at (a) $E_{\mathrm{lab}} = 16.2$ MeV and (b) $E_{\mathrm{lab}} = 21.3$ MeV, and the open circles are the experimental data from Majer *et al.* at $E_{\mathrm{lab}} = 16.8$ MeV [23].

In Fig. 4 we present our angular distributions compared with the data of Majer *et al.* [23]. The angular resolution of the present experiment was estimated by a Monte Carlo simulation to be of the order of $\Delta\theta_{\mathrm{lab}} \simeq 2.7^\circ$ ($1\ \sigma$). In this simulation we considered the effect of the geometry of the experiment, namely, the aperture of the detector collimators ($\pm 2.4^\circ$), the secondary beam spot size (2 mm), its intrinsic angular divergence ($\approx 3^\circ$), and the angular straggling in the ^{197}Au target ($\approx 1.2^\circ$) which was estimated by STOPX calculations [28]. The experimental angular resolution will eventually cause a damping of the oscillations in the angular distributions and its effect will be taken into account further when comparing the data with the calculations, as described in the next sections.

III. THEORETICAL ANALYSIS

A. CC calculations in a collective model

Besides the effects derived from the weak binding of the ^{6}He projectile, the dynamics of the ^{6}He + ^{9}Be reaction may be also affected by the couplings arising from the target excitation. The ^{9}Be nucleus has a large static quadrupole moment ($Q_2 = +4.9 \pm 0.3$ e fm^2) [29] that may induce important reorientation effects. In addition, its low-lying spectrum has a marked rotational structure. Quadrupole couplings between the $3/2^-$ ground state and the $5/2^-$ excited state at $E_x = 2.43$ MeV have been found to be very important in the ^{6}Li + ^{9}Be reaction at $E_{\rm c.m.} = 7$ MeV and their inclusion within a CC calculation improved significantly the description of the elastic scattering angular distribution with respect to a single-channel calculation performed with a double-folding potential [24]. Given the similitude between both reactions, we expect these couplings to be also important in the ^{6}He + ^{9}Be reaction.

Furthermore, the same authors found that the ^{6}Li + ^{9}Be elastic scattering is influenced by the coupling to the narrow 3^+ resonance of ^{6}Li at $E_x = 2.186$ MeV. In the ^{6}He nucleus, it is also expected that the low-lying 2^+ ($E_x = 1.8$ MeV) can be strongly excited in the reaction and affects the scattering observables.

We have thus performed CC calculations including simultaneously the couplings due to the low-lying rotational states of ^{9}Be and the 2^+ low-lying resonance of ^{6}He. An essential ingredient of the CC calculations is the bare potential between the projectile and the target, i.e., the interaction between them in the absence of couplings to their internal degrees of freedom. For the real part of this bare interaction we have used the São Paulo potential (SPP) [30,31]. This is a microscopic potential obtained by means of a double-folding procedure, using the matter densities of the colliding nuclei and an effective nucleon-nucleon interaction, multiplied by an energy-dependent term, which accounts for part of the nonlocality of the optical potential. For the imaginary part of the bare interaction we use a volume Woods-Saxon potential with the same geometry used by Muskat *et al.* [24] for ^{6}Li + ^{9}Be ($r_i = 2.81$ fm, $a_i = 0.6$ fm) and depth $W_0 = 4.0$ MeV (for $E_{\rm lab} = 16.2$ and 21.3 MeV).

Besides the ground state and the $5/2^-_1$ excited state of ^{9}Be considered in Ref. [24], we include also the $7/2^-_1$ excited state at $E_x = 6.38$ MeV. These three states are assumed to belong to a $K = 3/2$ rotational band. Diagonal (reorientation) and nondiagonal couplings between these states are generated by deforming the bare potential using the quadrupole deformation length $\delta_2 = 2.9$ fm, derived in Ref. [24] from the $B(E2)$ value for the $\frac{3}{2}^- \rightarrow \frac{5}{2}^-$ transition. The calculations were performed with the code FRESCO [32].

In Fig. 5, we compare the measured elastic differential cross section (relative to Rutherford) with the CC calculations. The top and bottom panels correspond to $E_{\rm lab} = 16.2$ and 21.3 MeV, respectively. In each panel, the dotted line is the one-channel calculation performed with the bare interaction alone. This calculation roughly reproduces the positions of the maxima and minima of the data, but the oscillations are too pronounced. Including the coupling to the ^{6}He 2^+_1 resonance and the ^{9}Be collective states cited above (dashed line), these oscillations are damped and the agreement with the data is improved. A CC calculation considering only the 2^+ state of the ^{6}He has shown that the coupling to this state is dominant and the effect of the coupling to the ^{9}Be low-lying states is very small.

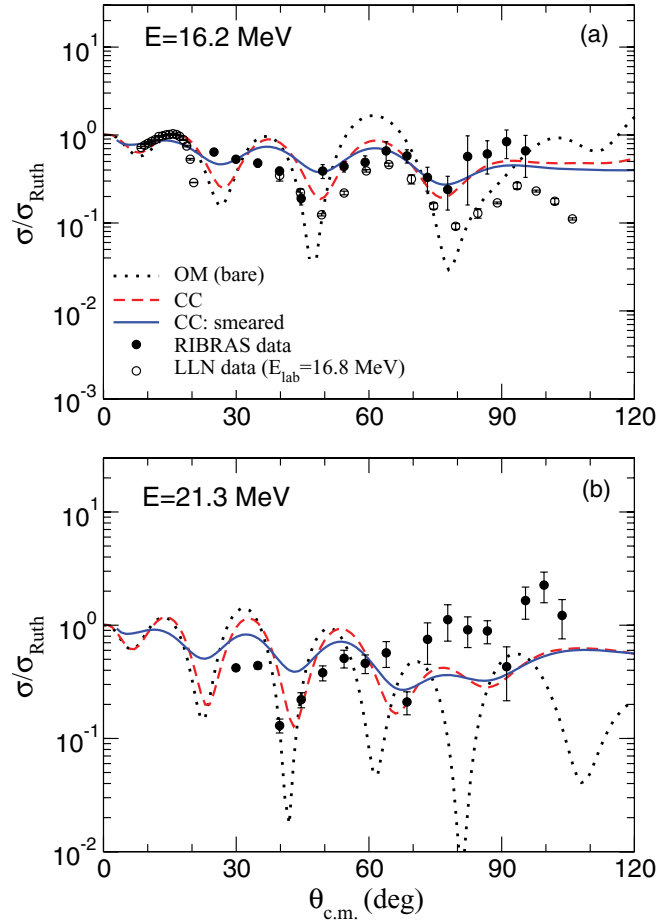

FIG. 5. (Color online) Elastic scattering angular distribution for ^{6}He + ^{9}Be at (a) $E_{\rm lab} = 16.2$ MeV and (b) $E_{\rm lab} = 21.3$ MeV. The solid circles are the data from the present experiment and the open circles (top panel) are the experimental data from Majer *et al.* [23]. The dotted line is the optical model calculation performed with the bare interaction. The dashed line is the CC calculation, including the coupling to the 2^+_1 resonance in ^{6}He and some states of the target, as described in the text. The solid line corresponds to the same calculation, convoluted with the experimental angular resolution.

For a meaningful comparison with the data, the CC calculations have been convoluted with the experimental resolution $\Delta\theta_{\rm c.m.} \simeq 4.4^\circ$ ($1\ \sigma$). This convolution (solid line) produces an additional damping of the oscillations, improving the agreement with the data. However, at small angles ($\theta_{\rm c.m.} \approx 30^\circ$) the calculation does not reproduce the shape and magnitude of the data. Moreover, for $E_{\rm lab} = 21.3$ MeV the calculation underestimates the experimental cross section around 90°.

The results of this section clearly show that the excitation of the projectile has a significant influence on the reaction dynamics. In the next sections, we study in more detail the

role of the few-body degrees of freedom of the ^{6}He nucleus using the CDCC method.

B. Three-body CDCC calculations

Although an accurate treatment of the present reaction would require a three-body model of the ^{6}He system, it has been shown in several works [5,6,23] that a simple dineutron model of this nucleus, comprising an α core and a structureless dineutron cluster, may provide a reliable and simple description of these reactions. Following Ref. [6], the interaction between the two clusters is described with a Woods-Saxon shape, with $R = 1.9$ fm and $a = 0.39$ fm. For $\ell = 0$ states, the depth of this potential is adjusted to give the effective separation energy of 1.6 MeV between the two clusters. It was shown in Ref. [6] that the use of this value, instead of the two-neutron separation energy ($S_{2n} = 0.97$ MeV), provides a more realistic rms radius of the ground-state wave function. For $\ell = 2$, the intercluster potential is adjusted to reproduce the position of the 2^+ resonance ($E_x = 1.8$ MeV). Continuum states with $\ell = 0$–4 were included in the calculations. For $\ell = 1, 3, 4$, we simply took the depth obtained for $\ell = 0$. For each partial wave, the two-body continuum is truncated at a maximum excitation energy of $\varepsilon = 14$ MeV and discretized into 10 energy bins for each ℓ, evenly spaced in the linear momentum.

For the $\alpha + {}^9$Be interaction we took the optical potential from Taylor *et al.* [33]. In that work it was shown that the $\alpha + {}^9$Be elastic scattering is only well reproduced when a spin-orbit component is included in the optical model potential. Since the CC code used in the present calculations does not allow the inclusion of noncentral components in the fragment-target interactions, we have considered this interaction approximately, adding a spin-orbit component acting on the ^{6}He-^{9}Be relative coordinate. Note that in these calculations possible effects arising from target excitation are not considered explicitly, but they are effectively taken into account by the fragment-target optical potentials.

For the $2n + {}^9$Be interaction, we used the following single-folding model:

$$U(\mathbf{R}) = \int d\mathbf{r}_{nn}\rho_{nn}(r_{nn})\left[U_n\left(\mathbf{R} + \frac{\mathbf{r}_{nn}}{2}\right) + U_n\left(\mathbf{R} - \frac{\mathbf{r}_{nn}}{2}\right)\right], \tag{2}$$

where U_n is the neutron-^{9}Be optical potential taken from the parametrization of Dave and Gould [34], evaluated at the appropriate energy per nucleon, and $\rho_{nn}(r)$ is the neutron-neutron density distribution. The latter was calculated averaging the square of the three-body wave function of the ^{6}He nucleus along the $2n$-α coordinate, i.e.,

$$\rho(r_{nn}) = r_{nn}^2 \int |\Psi^{3b}(\mathbf{r}_{nn}, \mathbf{r}_{2n\text{-}\alpha})|^2 d\mathbf{r}_{2n\text{-}\alpha} d\Omega_{nn}, \tag{3}$$

where $\Psi^{3b}(\mathbf{r}_{nn}, \mathbf{r}_{2n\text{-}\alpha})$ is the three-body wave function and Ω_{nn} denotes the angular variables (θ_{nn}, ϕ_{nn}). In the present calculations, the function Ψ^{3b} was taken from Ref. [6].

The results of the three-body CDCC (3b-CDCC) calculations are shown by dashed lines in Fig. 6. The top and bottom panels correspond to $E_{\rm lab} = 16.2$ and 21.3 MeV, respectively. The dotted line is the one-channel calculation, in which continuum couplings are omitted. The difference between the one-channel and full calculations evidences the significant effect of the coupling to the ^{6}He breakup channels. Although the coupling potentials used in the CDCC calculations include both nuclear and Coulomb couplings, we have verified that the effect of the Coulomb breakup is negligible. Therefore, the difference between the one-channel and the full calculation is almost entirely due to nuclear couplings.

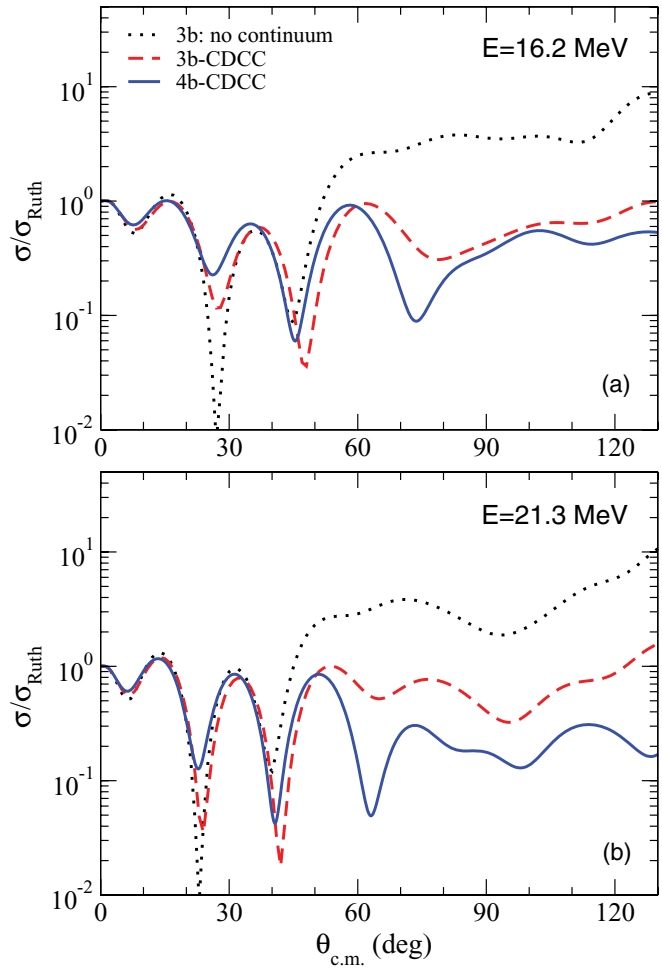

FIG. 6. (Color online) Elastic scattering angular distributions for ^{6}He + ^{9}Be at (a) $E_{\rm lab} = 16.2$ MeV and (b) $E_{\rm lab} = 21.3$ MeV. In both panels, the dashed line corresponds to the 3b-CDCC calculation and the solid line to the 4b-CDCC calculation. The dotted line is the 3b-CDCC calculation omitting the coupling to the continuum.

In Fig. 7 we compare the full 3b-CDCC calculation and the calculation omitting the continuum, both convoluted with the experimental angular resolution, with the experimental data. Overall, the calculation reproduces well the shape of the data. It is also apparent that the inclusion of the coupling to the ^{6}He continuum is essential to explain the shape and magnitude of the data. At smaller angles, the one-channel calculation exhibits pronounced minima not observed in the data, whereas at larger angles it largely overestimates the experimental points. Although full convergence of the elastic

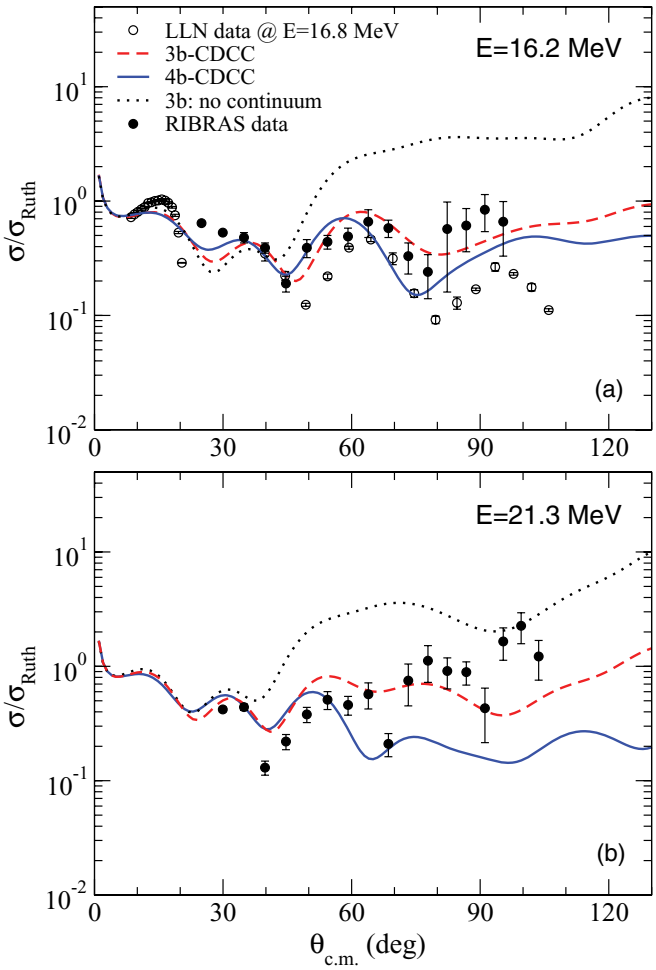

FIG. 7. (Color online) Elastic scattering angular distribution for ^{6}He + ^{9}Be at (a) $E_{\rm lab} = 16.2$ MeV and (b) $E_{\rm lab} = 21.3$ MeV. The solid circles are the data from the present experiment and the open circles (top panel) are the experimental data from Majer *et al.* [23] for $E_{\rm lab} = 16.8$ MeV. The dashed and solid lines correspond to the 3b- and 4b-CDCC calculations, respectively, convoluted with the experimental angular resolution. The dotted lines are the 3b-CDCC calculations omitting the coupling to the continuum, also convoluted with the experimental angular resolution.

cross section requires the inclusion of $2n$-α partial waves up to $\ell = 4$, we found that most of the effect comes from the nuclear couplings to the 2^+ continuum states and, in particular, to the low-lying resonance at $E_x = 1.8$ MeV. This is in contrast with the situation with heavy targets where the main effect arises from the coupling to the 1^- continuum states due to the dipole Coulomb interaction [5].

Despite the reasonable agreement between the full 3b-CDCC calculation and the data, some differences remain at both energies. At $E_{\rm lab} = 16.2$ MeV, the calculation predicts a minimum around 25°, whereas the data are almost flat. At $E_{\rm lab} = 21.3$ MeV, the calculation underpredicts the last three data points. Part of this disagreement could be due to the limitations of the dineutron model used in these calculations. In the following section, we present four-body CDCC (4b-CDCC) calculations based on a more realistic three-body model of the ^{6}He nucleus.

C. Four-body CDCC calculations

As mentioned above, an appropriate treatment of reactions induced by the Borromean nucleus ^{6}He requires a four-body formalism (three-body projectile plus a target). This is possible within the CDCC framework that has been recently extended to four-body problems [7–11]. Among the different discretization methods developed to treat the continuum of the three-body projectile we have chosen here the transformed harmonic oscillator (THO) [35], used within the CDCC framework in previous works [4,9,10,36].

The structure model used is the same as that in Refs. [9,10,35], obtaining a ground state with calculated binding energy of 0.95 MeV and a rms point nucleon matter radius of 2.46 fm, when assuming an α-particle rms matter radius of 1.47 fm. We have taken into account the states with total angular momentum $j = 0^+, 1^-, 2^+$ up to a maximum energy $\varepsilon_{\rm max} = 14$ MeV for both incident energies. This means that we need to include closed channels ($\varepsilon > 8.77$ and 11.83 MeV for $E_{\rm lab} = 16.2$ and 21.3 MeV, respectively) to get convergence of the elastic cross section. The effect of higher j is negligible in this model for these reactions. We have studied the convergence with the size of the THO basis, including states up to $n = 6$ of oscillator number. The coupled equations are solved with the code FRESCO that reads externally the coupling potentials. To have a fair comparison with the 3b-CDCC calculations, the optical potentials used for the interactions between the fragments of the projectile and the target are the same as those in the preceding subsection. We solved the coupled equations up to $J = 40$ partial waves and matching with asymptotic solutions at $R_{\rm match} = 30$ fm.

The results for the elastic cross-section distribution are shown in Figs. 6 and 7 with solid lines. In the latter, the experimental data are included and, accordingly, the calculations have been convoluted with the experimental angular resolution. The calculation omitting the continuum within this four-body model is practically indistinguishable from the 3b-CDCC calculation without the continuum.

We see that the agreement between the data and the full 4b-CDCC calculation is very good for the reaction at $E_{\rm lab} = 16.2$ MeV, whereas for the reaction at $E_{\rm lab} = 21.3$ MeV the calculation underestimates the data at backward angles, as found with the collective model and with the dineutron model to a lesser extent.

It is noticeable also that the 3b- and 4b-CDCC calculations present some differences, in contrast to the results found in Ref. [6], where both models predicted very similar results for all the targets and energies analyzed. A possible reason for this is that the calculations of Ref. [6] correspond to heavier targets, where the Coulomb couplings (in particular dipole ones) become more important [37]. It was shown in that work that the improved dineutron model used here accounts well for the $B(E1)$ and $B(E2)$ distributions predicted by a three-body model. However, in the present work, where we deal with a light target, the effect of the continuum on the elastic scattering

is likely dominated by nuclear couplings. It would be desirable to study the reliability of the dineutron model proposed in Ref. [6] to these nuclear-dominated situations.

D. Trivial local polarization potential

The analysis in the preceding sections demonstrates that the coupling to the ^{6}He breakup channels plays an important role in the reaction dynamics. The effect of channel couplings can be characterized in terms of a polarization potential, that is, an effective interaction that simulates the overall effect of these couplings on the elastic scattering. It has been shown that, for the scattering of a weakly bound system by a light target [12,14], this polarization potential is characterized by a repulsive real part and a long-range imaginary part. For the scattering of ^{6}He on a heavy target, in addition to these long-range components, the polarization potential contains also an attractive real part of long range, originated by the dipole part of the Coulomb interaction [36]. It is then illustrative to study these features in a light target, like ^{9}Be. In the present work, the polarization potential has been generated using the prescription of Thompson *et al.* [38], which involves two steps. First, for each total angular momentum, a local polarization potential is calculated from the source term of the elastic channel equation. Then, an L-independent potential is constructed by averaging these L-dependent polarization potentials, weighted with the breakup cross section for each angular momentum. The calculated potential, referred to as *trivial local polarization* (TLP) potential, can be regarded as a simplified local approximation of a complicated CC system.

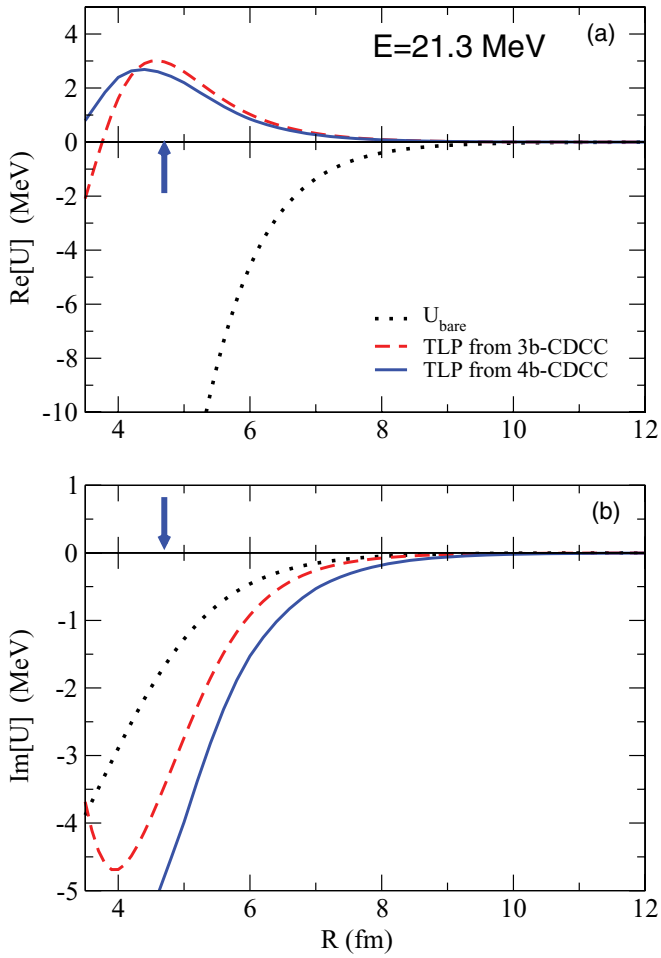

FIG. 8. (Color online) TLP potential extracted from the 3b- and 4b-CDCC calculations for ^{6}He + ^{9}Be at $E_{lab} = 21.3$ MeV with dashed and solid lines, respectively. The top (a) and bottom (b) panels correspond to the real and imaginary parts. The dotted line in each panel is the Watanabe-like potential obtained by folding the sum of the $2n$-^{9}Be and α-^{9}Be interactions with the ground-state density of ^{6}He, calculated in a dineutron cluster model.

In Fig. 8 we display the TLP calculated for the ^{6}He + ^{9}Be potential at 21.3 MeV extracted from the 3b-CDCC (dashed lines) and 4b-CDCC (solid lines) calculations. The top and bottom panels correspond to the real and imaginary parts. For comparison, in this graph we include also the one-channel potential (dotted line), defined as the sum of the $2n$-^{9}Be and α-^{9}Be interactions, folded with the ground-state density of the ^{6}He nucleus. The arrows denote the sum of the radii of the colliding nuclei, $R = R_1 + R_2$. Qualitatively, the TLPs from the 3b- and 4b-CDCC calculations exhibit the same behavior. The real part is repulsive at distances around this radius, whereas the imaginary part has a diffuse tail and extends to distances significantly larger than the one-channel potential. These features are very similar to those found for the scattering of other weakly bound systems from light targets, where Coulomb effects are small [12,14]. This result confirms our conclusions that, for these light systems, the reaction dynamics is dominated by nuclear effects. Despite their qualitative agreement, the imaginary part of the TLP derived from the 4b-CDCC calculation extends to larger distances, which might explain the differences in the elastic scattering with the 3b-CDCC for this reaction.

IV. SUMMARY AND CONCLUSIONS

We have presented new data for the ^{6}He + ^{9}Be reaction at 16.2 and 21.3 MeV obtained at the RIBRAS facility from the University of São Paulo.

The effect of the target excitation has been investigated by means of CC calculations, including the coupling to the first three members of the ground-state rotational band of the ^{9}Be nucleus. In addition, coupling to the 2_1^+ resonance of ^{6}He was also included, assuming also a collective model with a deformation length extracted from the literature [39]. To reduce the number of adjustable parameters, the projectile-target bare interaction has been described by means of the São Paulo double-folding potential, supplemented with an imaginary part, taken from a previous analysis of the ^{6}Li + ^{9}Be reaction at a similar energy. The coupling to the 2_1^+ resonance of ^{6}He has been found to affect significantly the reaction dynamics, improving considerably the agreement with the data with respect to the single-channel calculation performed with the bare interaction alone. The coupling to the target excitations has a minor effect in the angular range of the elastic distributions analyzed here.

Three-body and four-body CDCC calculations have been also performed to study the role of the few-body degrees of freedom of the ^{6}He on the reaction. These effects are found also to play a significant role and are dominated by the nuclear couplings to 2^+ continuum states and, in particular, with the low-lying resonance. This result is in contrast to the case of ^{6}He reactions with heavy targets, which are dominated by the Coulomb couplings to the dipole states [5]. In addition, the trivial local polarization potential extracted from the 3b- and 4b-CDCC calculations exhibits the long-range absorption effect found for heavier targets, although the imaginary tail is mainly due to the nuclear couplings. Therefore, our calculations corroborate previous findings indicating that couplings to breakup channels are still important in ^{6}He reactions by light targets, but the nature of these couplings is very different from that of heavy targets.

Although the 3b- and 4b-CDCC calculations yield similar results, we have found some nonnegligible differences between them. These differences might be due to the limitations of the dineutron model for a genuine three-body system like ^{6}He, but also to the numerical difficulties inherent in the 4b-CDCC calculations. These differences should be further investigated and, in this respect, accurate measurements of elastic data would provide a useful benchmark.

ACKNOWLEDGMENTS

We are grateful to R. Raabe for providing us with the ^{6}He + ^{9}Be data from Louvain-la-Nueve. K.C.C.P. acknowledges financial support by the Junta de Andalucía, FAPESP, and Banco Santander. This work has been partially supported by the Spanish Ministerio de Ciencia e Innovación under Projects FPA2009-07653 and PCI2006-A7-0654 and by the Spanish Consolider-Ingenio 2010 Programme CPAN (CSD2007-00042).

[1] O. R. Kakuee *et al.*, Nucl. Phys. A **728**, 339 (2003).
[2] O. R. Kakuee *et al.*, Nucl. Phys. A **765**, 294 (2006).
[3] A. M. Sánchez-Benítez *et al.*, Nucl. Phys. A **803**, 30 (2008).
[4] P. N. de Faria *et al.*, Phys. Rev. C **81**, 044605 (2010).
[5] K. Rusek, I. Martel, J. Gómez-Camacho, A. M. Moro, and R. Raabe, Phys. Rev. C **72**, 037603 (2005).
[6] A. M. Moro, K. Rusek, J. M. Arias, J. Gómez-Camacho, and M. Rodríguez-Gallardo, Phys. Rev. C **75**, 064607 (2007).
[7] T. Matsumoto, E. Hiyama, K. Ogata, Y. Iseri, M. Kamimura, S. Chiba, and M. Yahiro, Phys. Rev. C **70**, 061601(R) (2004).
[8] T. Matsumoto, T. Egami, K. Ogata, Y. Iseri, M. Kamimura, and M. Yahiro, Phys. Rev. C **73**, 051602(R) (2006).
[9] M. Rodríguez-Gallardo, J. M. Arias, J. Gómez-Camacho, R. C. Johnson, A. M. Moro, I. J. Thompson, and J. A. Tostevin, Eur. Phys. J. S. T. **150**, 51 (2007).
[10] M. Rodríguez-Gallardo, J. M. Arias, J. Gómez-Camacho, R. C. Johnson, A. M. Moro, I. J. Thompson, and J. A. Tostevin, Phys. Rev. C **77**, 064609 (2008).
[11] M. Rodríguez-Gallardo, J. M. Arias, J. Gómez-Camacho, A. M. Moro, I. J. Thompson, and J. A. Tostevin, Phys. Rev. C **80**, 051601(R) (2009).
[12] N. Austern, Y. Iseri, M. Kamimura, M. Kawai, G. Rawitscher, and M. Yahiro, Phys. Rep. **154**, 125 (1987).
[13] M. Yahiro, Y. Iseri, H. Kameyama, M. Kamimura, and M. Kawai, Prog. Theor. Phys. Suppl. **89**, 32 (1986).
[14] Y. Sakuragi, Phys. Rev. C **35**, 2161 (1987).
[15] M. Takashina, S. Takagi, Y. Sakuragi, and Y. Iseri, Phys. Rev. C **67**, 037601 (2003).
[16] A. N. Ostrowski *et al.*, J. Phys. G **24**, 1553 (1998).
[17] I. Krouglov and W. von Oertzen, Eur. Phys. J. A **8**, 501 (2000).
[18] M. Milin *et al.*, Nucl. Phys. A **730**, 285 (2004).
[19] R. J. Smith, J. J. Kolata, K. Lamkin, A. Morsad, K. Ashktorab, F. D. Becchetti, J. A. Brown, J. W. Janecke, W. Z. Liu, and D. A. Roberts, Phys. Rev. C **43**, 761 (1991).
[20] C. Tao *et al.*, Chin. Phys. Lett. **19**, 921 (2002).
[21] K. Lukyanov, V. Lukyanov, E. Zemlyanaya, A. Antonov, and M. Gaidarov, Eur. Phys. J. A **33**, 389 (2007).
[22] E. A. Benjamim *et al.*, Phys. Lett. B **647**, 30 (2007).
[23] M. Majer *et al.*, Eur. Phys. J. A **43**, 153 (2010).
[24] E. Muskat, J. Carter, R. W. Fearick, and V. Hnizdo, Nucl. Phys. A **581**, 42 (1995).
[25] R. Lichtenthäler *et al.*, Eur. Phys. J. A **25**, 733 (2005).
[26] K. C. C. Pires, I. Mukha, A. M. Moro, R. Lichtenthäler, and J. Gómez-Camacho, AIP Conf. Proc. **1231**, 173 (2010).
[27] K. C. C. Pires *et al.*, in CERN-Proceedings-2010-001, 12th International Conference on Nuclear Reaction Mechanisms, 2010.
[28] W. T. Milner, VAXPAK Package, 1987.
[29] A. G. Blachman and A. Lurio, Phys. Rev. **153**, 164 (1967).
[30] L. C. Chamon, B. V. Carlson, L. R. Gasques, D. Pereira, C. De Conti, M. A. G. Alvarez, M. S. Hussein, M. A. Cândido Ribeiro, E. S. Rossi, and C. P. Silva, Phys. Rev. C **66**, 014610 (2002).
[31] L. C. Chamon, D. Pereira, M. S. Hussein, M. A. Cândido Ribeiro, and D. Galetti, Phys. Rev. Lett. **79**, 5218 (1997).
[32] I. Thompson, Comp. Phys. Rep. **7**, 167 (1988).
[33] R. B. Taylor, N. R. Fletcher, and R. H. Davis, Nucl. Phys. **65**, 318 (1965).
[34] J. H. Dave and C. R. Gould, Phys. Rev. C **28**, 2212 (1983).
[35] M. Rodríguez-Gallardo, J. M. Arias, J. Gómez-Camacho, A. M. Moro, I. J. Thompson, and J. A. Tostevin, Phys. Rev. C **72**, 024007 (2005).
[36] J. P. Fernandez-Garcia, M. Rodriguez-Gallardo, M. A. G. Alvarez, and A. M. Moro, Nucl. Phys. A **840**, 19 (2010).
[37] M. Hussein, R. Lichtenthäler, F. Nunes, and I. Thompson, Phys. Lett. B **640**, 91 (2006).
[38] I. J. Thompson, M. A. Nagarajan, J. S. Lilley, and M. J. Smithson, Nucl. Phys. A **505**, 84 (1989).
[39] T. Aumann *et al.*, Phys. Rev. C **59**, 1252 (1999).